J. Fluid Mech. (1984), *vol.* 139, *pp.* 391–416
Printed in Great Britain

Velocity characteristics in the turbulent near wakes of confined axisymmetric bluff bodies

By A. M. K. P. TAYLOR AND J. H. WHITELAW
Mechanical Engineering Department, Fluids Section, Imperial College of Science and Technology, London SW7 2BX

(Received 17 January 1983 and in revised form 17 October 1983)

Measurements of the velocity characteristics and wall pressure are reported for the axisymmetric turbulent flow downstream of three bluff bodies (disks of 25 % and 50 % area blockage and a cone of 25 % blockage) confined by a long pipe. The dimensions of the recirculation regions were found from the mean-velocity components, which were determined by a laser-Doppler velocimeter: the corresponding components of Reynolds stress were also recorded. The lengths and maximum widths of the recirculation bubbles (in bluff-body diameters), recirculating mass-flow rates (normalized by the average velocity in the plane of the baffle, U_0, and the baffle diameter) and maximum turbulent kinetic energy (normalized by U_0^2) were as follows: cone 1.55, 0.55, 0.19, 0.11; disk (25 % blockage) 1.75, 0.62, 0.31, 0.19; disk (50 % blockage) 2.20, 0.55, 0.26, 0.16. The increase in recirculation length with blockage is opposite to the trend in unconfined, annular jets. The distribution of Reynolds stresses is strongly dependent on blockage: for the smaller blockage both the disk and the cone have the maximum value of kinetic energy near the rear stagnation point. It is proposed that this is because the generation of turbulence by normal stresses is more important in the flow consequent on the smaller blockage.

The measurements include profiles of the velocity characteristics at, as well as upstream of, the trailing edges of the baffles for use as boundary conditions in numerical solutions of the equations of motion.

1. Introduction

The separated recirculating flow which is established in the lee of bluff bodies ('baffles') can be used to stabilize flames in high-velocity reactant streams. The details of the aerodynamics of the near wake are crucial to the description of the mechanism of stabilization. For example, the size of the recirculation zone affects the rate of production of hot, burnt products, and the mixing between these products and the reactants is governed by the turbulence in the free shear layers.

The study of isothermal models of the combusting flow allows much to be learnt about the near wake in experimentally, and conceptually, simpler flows. This paper presents measurements of the mean and fluctuating velocity components for three (separate) confined axisymmetric baffles, and quantifies the influence of baffle diameter and shape.

Measurements of recirculation length and base pressure are available for a wide variety of baffle cross-sections and forebody shapes (e.g. Fail, Lawford & Eyre 1957; Calvert 1967; Humphries & Vincent, 1976*a*, *b*; Chigier & Gilbert 1968; Winterfeld, 1965; Sullerey, Gupta & Moorthy 1975). The accurate measurement of the instantaneous velocities in the near wake has been restricted by the unsuitability of the

hot-wire anemometer in highly turbulent reversed flows. Although many early references relied on this instrument (e.g. Carmody 1964), work by Bradbury (1976) has shown that the results can be qualitatively, as well as quantitatively, incorrect. The development of the pulsed-wire anemometer and laser-Doppler velocimeter has provided means with which to make reliable observations, with references on plane baffles (Bradbury 1976; Fujii, Gomi & Eguchi 1978) and axisymmetric and asymmetric annular jets (Durão & Whitelaw 1978; Durão, Founti & Whitelaw 1979). These instruments have also been applied in the study of separated flows in which the separation streamline reattaches to a solid surface (e.g. Etheridge & Kemp 1978; Moss, Baker & Bradbury 1977; Smyth 1979; Castro & Robbins 1977).

This paper is concerned with the turbulent flow over a baffle in a long pipe, with three separate baffles being investigated: a disk presenting an area blockage to the approaching stream of 25%, a cone of 25% area blockage ratio and a disk of 50% blockage ratio. The velocity characteristics have been measured with a laser-Doppler velocimeter. The work is related to that of Durão & Whitelaw (1976), which was concerned with annular jets – in other words flows *without* confinement downstream of the baffle.

The choice of these three baffles allows the comparative study of the influence of the baffles' forebody shape and area blockage ratio on the size of the recirculation zone, the magnitude of the recirculating mass flow rate and the field distributions of the Reynolds stresses. A further purpose in making these measurements is to provide accurate detailed observations for the evaluation, in recirculating flows, of numerical solutions of the equations of motion which use turbulence models. In such calculations, it is desirable to know, from experiment, the flow conditions at a boundary which lies either at, or upstream of, the trailing edge of the baffle.

The measurement of velocity in this region was therefore a major objective, and its acquisition represents an important advance, from the point of view of those interested in testing calculation methods, over previous publications.

Section 2 gives details of the experimental method, and describes the flow configuration, the laser-Doppler velocimeter and the errors incurred in the measurements. Section 3 presents the mean velocities and Reynolds stresses for each baffle, and this is followed, in §4, by discussion of the influence of the forebody shape and blockage, and the effect of confinement downstream of the baffle. Section 5 presents a summary of the main findings and conclusions.

2. Experimental method

2.1. *Flow configuration*

The baffles, which are described below, were inserted in a water tunnel with a working section made of a length of Perspex pipe (50.3 ± 0.5 mm bore, 5 mm wall thickness). This pipe extended for 22 hydraulic diameters both upstream and downstream of the baffle. The flow was driven by the pressure difference between a constant head and a discharge tank. Optical access (for the laser-Doppler velocimeter) to the working section was improved by immersing the section in a plane-walled water trough.

Two forebody shapes of the baffle were chosen: a disk and a cone of 45° included angle, both of which presented an area blockage ratio of 25%. The influence of blockage was examined with a disk of 50% area blockage ratio. The details of the three baffles are illustrated on figure 1. The origin of the axial (x) and radial (r) coordinates in the pipe is taken at the centre of the downstream face of the baffles.

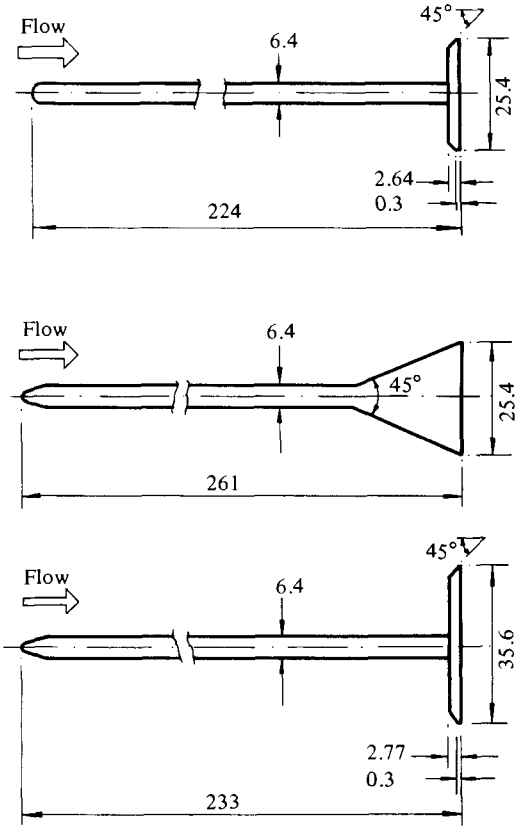

All dimensions in mm

FIGURE 1. Shapes and dimensions of baffles.

	Area blockage ratio (%)	Annular bulk† velocity (m/s)	Reynolds number‡
Disk	25	1.37	34700
Cone	25	1.53	38900
Disk	50	1.62	57700

† Annular bulk velocity refers to bulk velocity (U_0) at the trailing edge of the baffle.
‡ The Reynolds number is based on the annular bulk velocity and the diameter of the baffle.

TABLE 1. Blockage, bulk velocity and Reynolds number for the three bluff bodies

The flow conditions and the Reynolds numbers for each baffle are summarized in table 1.

Each baffle was positioned by four radial pylons abutting against the sting upstream of each baffle. The pylons were thin streamlined plates, and the accuracy with which each baffle could be centred was limited only by the lack of roundness in the pipe.

5 mW He–Ne laser	632.8 nm
Focal length of lenses:	
imaging lens from laser to grating	150 mm (nominal)
collimating lens after grating	300 mm (nominal)
imaging lens to form measuring volume	200 mm (nominal)
Beam diameter, at e^{-2} intensity, of laser	0.65 mm
Measured half-angle of intersection (in air)	9.09°
Calculated half-angle of intersection (in water)	6.82°
Fringe separation (line pair spacing)	2.003 μm
Calculated dimensions of measuring volume (in water):	
minor axis to e^{-2} intensity	0.13 mm
major axis to e^{-2} intensity	1.34 mm
Calculated number of fringes within e^{-2} intensity level	63
Velocimeter transfer constant	0.499 MHz/(m s^{-1})
Shift frequency (nominal)	1.8 MHz
Short-term stability of shift frequency (r.m.s.)	0.2 %

TABLE 2. Principal characteristics of the laser-Doppler velocimeter

2.2. *Measurement technique*

The laser-Doppler velocimeter operated in the symmetric heterodyne ('dual-beam'), forward scatter, individual-realization mode with light frequency shifting (see e.g. Durst, Melling & Whitelaw 1981) provided by the steady rotation of a radial diffraction grating (manufactured by the Technische Physische Dienst, tno-th, Holland: type 'H'). The principal characteristics of the laser-Doppler velocimeter are summarized in table 2.

The light scattered by naturally occurring centres in the water was detected by a photomultiplier tube (E.M.I. 9558) and the Doppler frequency of the signal was demodulated by a frequency tracker (Cambridge Consultants CC01). The output of the tracker (a voltage proportional to the magnitude of the Doppler frequency) was time-averaged to give the mean and root-mean-square values of velocity.

The mean and variance ($U, \langle u^2 \rangle$) of the axial component of velocity were obtained by making measurements in a plane containing the pipe's axis. No correction to the transfer constant of the velocimeter (Doppler frequency to velocity), due to the effects of refraction at the pipe (or water trough) walls, is necessary. The radial ($V, \langle v^2 \rangle$) and azimuthal ($\langle w^2 \rangle$) components were obtained in the plane of the cross-section of the pipe, and allowance has to be made for refraction effects. The position of the measuring volume and the changes in the transfer constant were calculated by an extension of the analysis of Kirmse (1974) and were found to be typically about 1 % of the undisturbed value. Despite the presence of the water trough, the measurement of the radial component became progressively more difficult as the pipe wall was approached, because of the increasing refraction at solid–liquid interfaces. The farthest position at which values could be reliably obtained was about $0.8r/R$ (where R is the pipe radius), and some data away from the pipe axis have been deleted from the presentation of the results below on the grounds that these were unreliable. It is emphasized that the axial and azimuthal components are unaffected by this consideration.

Wall-pressure measurements were made with a water micromanometer by means of wall-pressure tappings.

	Systematic error	Random error
U, V	$0.04U_0$	$\pm 2\%$
$\frac{\langle u^2\rangle}{U_0^2}, \frac{\langle v^2\rangle}{U_0^2}, \frac{\langle w^2\rangle}{U_0^2}$	< 0.003	$\pm 2\%$ to $\pm 6\%$
$\frac{k}{U_0^2}$	< 0.005	$\pm 2\%$ to $\pm 7\%$
$\frac{p}{\frac{1}{2}\rho U_0^2}$	0.003	± 0.003
x	0.25 mm	± 0.02 mm
r	0.03 mm	± 0.03 mm
Velocimeter transfer constant	$< \frac{1}{2}\%$	nil

TABLE 3. Estimates of systematic and random errors in quantities measured

2.3. *Accuracy and precision*

Table 3 summarizes our estimates of the maximum inaccuracy (systematic error) and precision (random error) associated with each measurement presented in §3. Of the sources of non-turbulent Doppler ambiguity (George & Lumley 1973), the largest is due to gradients of mean velocity across the measuring volume. The effects are included as systematic errors in the table for regions of high velocity gradients, such as near the pipe walls or close to the baffle: the systematic error is smaller away from such regions.

3. Results

The results are considered under two headings: the first presents profiles of mean velocity and derived quantities, and the second presents contours and profiles of Reynolds stresses. A detailed discussion of the results is reserved for §4.

Prior to the detailed measurements, stroboscopic visualization of hydrogen bubbles was used to guide the choice of measurement locations and to determine if the flow was subject to vortex shedding. No dominant frequencies were observed, and subsequent spectral analysis of Doppler signals confirmed that none existed.

3.1. *Profiles of mean velocity and wall pressure*

Figure 2 presents the radial profiles of axial velocity for axial stations upstream and downstream of the 25 % area-blockage-ratio disk. The first three profiles ($x = -0.84R$, $-0.20R$ and $+0.02R$) show how the flow accelerates towards the annular region formed at $x = 0$. The maximum in the profile at $x = 0.02R$ lies close to the baffle tip and, by analogy with the potential flow over a sphere, confirms that the flow upstream is dominated by the pressure field. The presence of the sting on the upstream face of the cone will not result in any important modifications to the flow: for the disks, a 'bound' recirculation zone will probably be present at the corner between the sting and the upstream face. It is unlikely, however, that this zone can be large because of the relatively small diameter of the sting and, by implication, the effects will be small also. The chamfer on the upstream face of the disks may give rise to flow separation upstream of the tip of the baffle. In any event, whatever the influence of

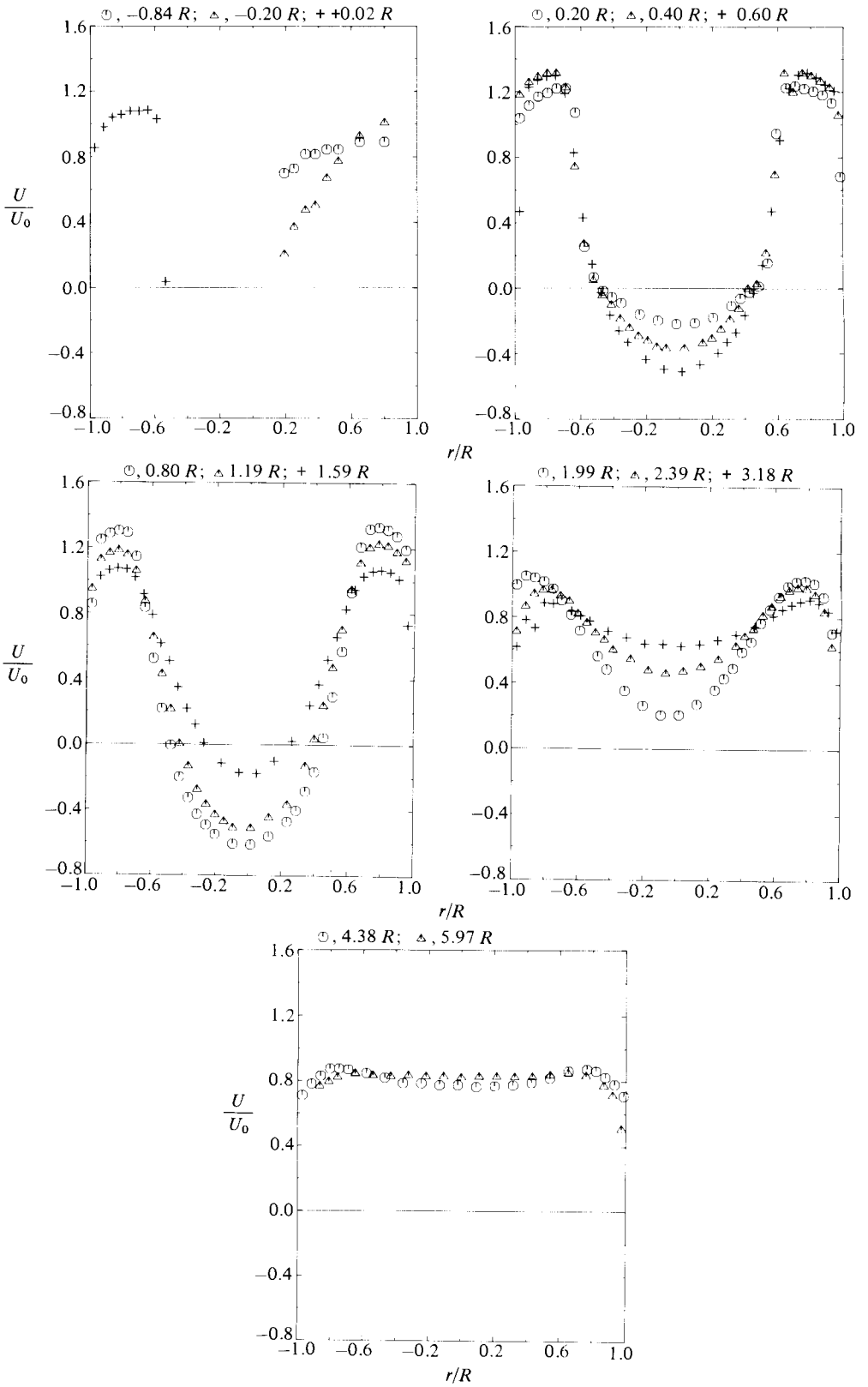

FIGURE 2. Disk, 25% blockage: radial profiles of axial velocity at successive axial stations ($U_0 = 1.37$ m/s, $R = 25.4$ mm).

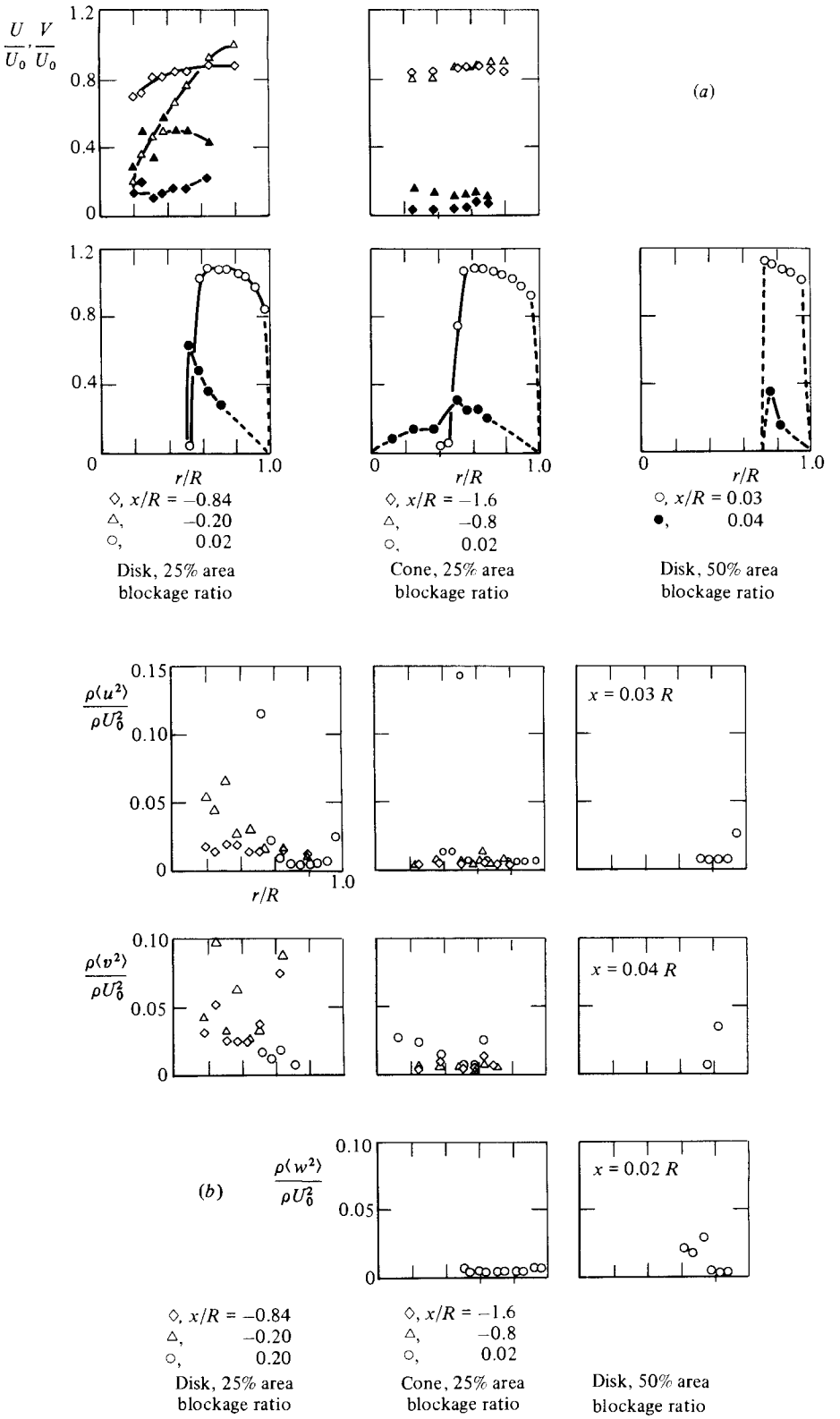

FIGURE 3. (*a*) Radial profiles of mean velocity upstream of and near the trailing edge of three bluff bodies. Open symbols are axial components; blocked are radial components. (*b*) Radial profiles of variance of velocity upstream of and near the trailing edge of three bluff bodies.

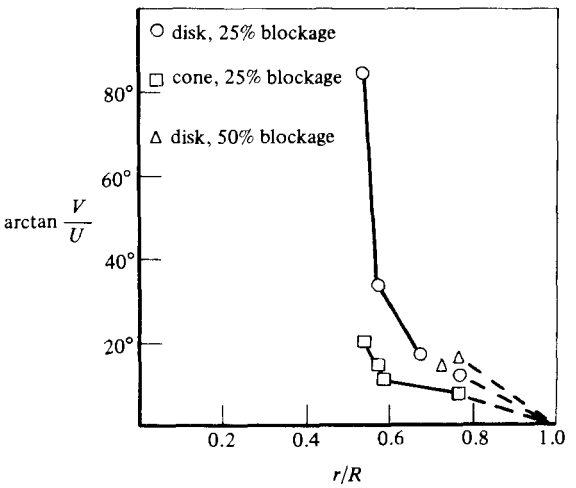

FIGURE 4. Comparison of streamline angles near the plane of the trailing edge of the three baffles.

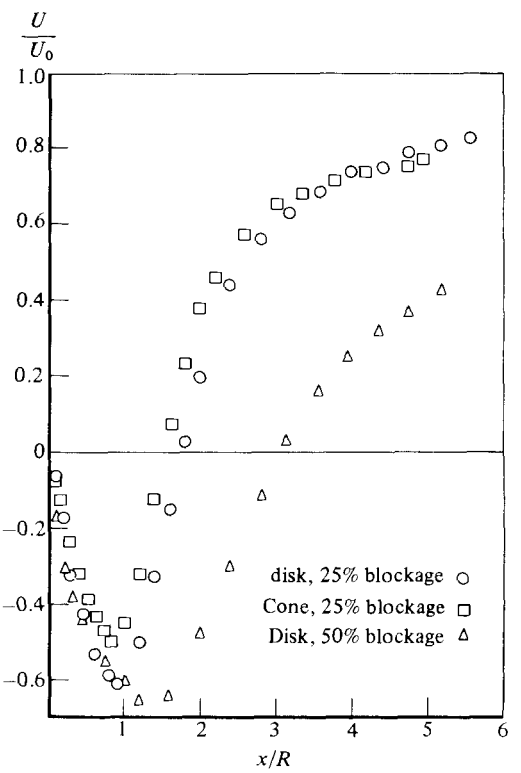

FIGURE 5. Centreline profiles of axial velocity for three baffles (lengthscale R is radius of confining pipe). Lengths of recirculation regions: disk, 25% blockage $1.75R$; cone $1.55R$; disk, 50% blockage $3.10R$.

the sting, or of the chamfer on the upstream face, the flow conditions at the plane of the trailing edge are quantified. Downstream of the baffle, profiles could be obtained over the whole width of the pipe, and figure 2 shows that asymmetries are small and within the positioning error of the measuring volume. The mass-flow rate was estimated by numerical integration of these profiles and the mean value was used

Authors	Flow type	Length†	Width†	$\frac{\dot{m}_r}{\dot{m}}$‡
This paper	Confined disk, 25% blockage	1.75	0.62	0.31
	Confined 45° cone, 25% blockage	1.55	0.55	0.19
	Confined disk, 50% blockage	2.20	0.55	0.26
Winterfield (1965)	Confined disk, 25% blockage	2.0	0.74	—
	Confined 90° cone, 25% blockage	1.9	0.64	—
	Confined 45° cone, 25% blockage	1.7	0.58	—
	Confined disk, 4% blockage	2.0	0.84	—
	Confined 90° cone, 4% blockage	1.9	0.72	—
	Confined 45° cone, 4% blockage	1.7	0.60	—
Fujii *et al.* (1978)	Confined 60° wedge, 50% blockage	1.88	0.59	0.10
Bradbury (1976)	Confined flat plate, 10% blockage	1.98	0.80	0.23
Davies & Béer (1971)	Annular jet, disk, 25% blockage	1.52	0.60	0.45
	Annular jet, 45° cone, 25% blockage	1.24	0.50	0.24
	Annular jet, cylinder, 25% blockage	0.72	0.50	—
	Annular jet, disk, 54% blockage	1.16	0.56	0.23
Durão & Whitelaw (1978)	Annular jet, disk, 20% blockage	1.45	—	—
	Annular jet, disk, 39% blockage	1.15	—	—
	Annular jet, disk, 50% blockage	1.00	—	—
Carmody (1964)	Unconfined disk (2% blockage)	2.5	0.85	0.25

† Lengths and widths expressed in baffle diameters or widths.

‡ $\dot{m}_r$ is the recirculating mass flow rate and $\dot{m} \equiv \frac{1}{4}\rho U_0 \pi d^2$ (where ρ is the density of the fluid, U_0 is the bulk velocity at the baffle's trailing edge) for axisymmetric baffles, or $\dot{m} \equiv \frac{1}{2}\rho U_0 b$ (where b is the baffle width) for plane flows.

TABLE 4. Size of the recirculation zone and recirculating mass-flow rate for various flows over bluff bodies

to calculate the bulk-flow velocity. The profiles downstream of the baffle resulted in flow rates within 5% of the mean.

Figure 3 summarizes the radial profiles of the velocity characteristics at, and (for the cone and 25% blockage disk) upstream of, the trailing edge of each baffle (the reader interested in detailed radial profiles of axial and radial velocity at other axial stations for the two remaining baffles is referred to Taylor (1981)). The profiles at two planes upstream of the trailing edge have been included for use by those who wish to begin calculations with these stations as upstream boundary conditions. The potential advantage to be had is that the outcome of the calculations is, doubtless, less sensitive to any experimental errors in the determination of the initial flow angles the farther upstream that this boundary is taken. The disadvantage of this strategy is that much numerical effort will have to be expended in representing the flow over the forebody of the baffles. The main result of decreasing the bluffness of the forebody shape from a disk to a cone is approximately to halve the values of radial velocity, with the result that the streamlines lie at a more shallow angle (figure 4). It is noted, however, that the angles near the tip of the larger disk are substantially smaller and this is due to the greater confinement.

The mean velocity characteristics downstream of the baffles can be easily compared by examining the centreline development of axial velocity (figure 5). The lengths x_r

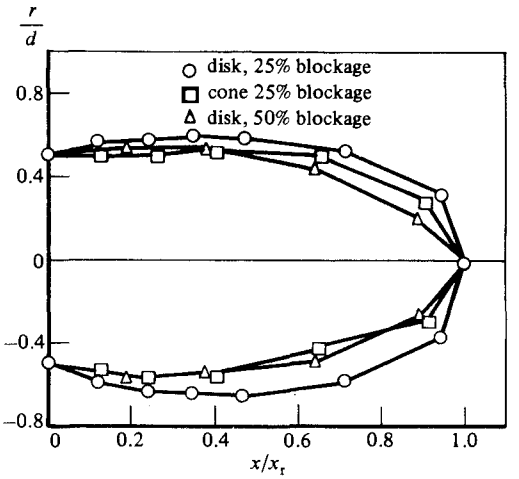

FIGURE 6. Comparison of the loci of the separation streamlines for the three baffles (lengthscales d and x_r are the baffle diameter and length of the recirculation zone respectively for each baffle).

of the recirculation zones, taken from this figure *but expressed in baffle diameters*, are given in table 4. It is noted that the 50% blockage disk gives rise to the longest recirculation bubble, irrespective of whether the confining pipe radius or the baffle diameter is used as a characteristic lengthscale. The mean trajectories of the separation streamlines are shown in figure 6, and have been constructed by evaluating the stream function from the measurements of axial velocity on each side of the geometric centreline, with the stream function defined as zero on the centreline. The ordinate has been normalized with the diameter d of each baffle, and the abscissa with x_r, so that the three separation streamlines originate and terminate at common points. The maximum width of the recirculation bubble associated with the cone is only 10% wider than the baffle that produces it, while that of the disk is wider by 24%. As expected from the results of figure 4, the width with the 50% blockage disk is comparatively smaller than that with the smaller disk.

The recirculating mass-flow rate $\dot{m}_r$ is another 'aggregate' quantity of the near wake which can be found from the calculated stream function. The values are given in table 4, normalized by $\dot{m}(\equiv \frac{1}{4}\rho U_0 \pi d^2)$. The magnitude of $\dot{m}_r$ is primarily dependent on the maximum values of the reversed velocity (figure 5) and recirculation bubble widths: as a consequence of the former dependence, the cone has only 0.6 the recirculating mass-flow rate of the comparable disk and, because of the latter, the smaller disk has 1.2 times that of the larger disk (in spite of the fact that the smaller disk has a smaller value of reversed velocity).

The flow outside the separation streamline must accelerate as it passes over the maximum width of the recirculation bubble (see figure 2). The fall in static pressure which accompanies this acceleration is shown on figure 7. For quantitative analysis, the value of the minimum pressure can be estimated by applying Bernoulli's equation to the flow outside the separation streamline. The assumptions which are made include being able to assign uniform values of pressure and velocity across the planes containing the trailing edge of the baffle and the maximum width of the recirculation bubble. Under such conditions, the minimum wall pressure p_m, is given by

$$\frac{p_m - p_0}{\frac{1}{2}\rho U_0^2} = 1 - \frac{(1-\alpha)^2}{(1 - W^2/R^2)^2}, \tag{1}$$

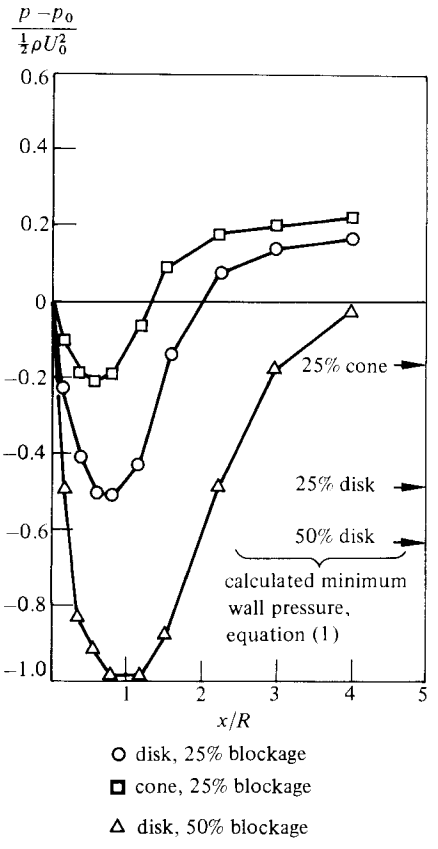

FIGURE 7. Axial variation of wall-pressure coefficient compared with analytical estimates for the minimum value (p_0 is wall pressure at $x/R = 0$).

where p_0 is the wall pressure at $x = 0$, α is the area blockage ratio of the baffle and W is the maximum width of the separation streamline. For the purposes of comparison, the value of p_m predicted by (1) is included on figure 7. The measurements confirm the expectation expressed by the equation: the agreement for the 50% blockage disk is fair considering that the sensitivity of p_m to even small errors in W is great.

3.2. *Distribution of Reynolds stresses*

The profiles of $\langle u^2 \rangle$, $\langle v^2 \rangle$ and $\langle w^2 \rangle$ are presented as contours of equal Reynolds stress, normalized by U_0^2. The contours have been drawn using linear interpolation between the measurements. The radial profiles from which the contours have been constructed are to be found in Taylor (1981).

Disc, 25% blockage

The contours of each component (figure 8) indicate that the recirculation bubble is a region of intense generation of turbulence, followed by dissipation downstream. The large increase in $\langle u^2 \rangle$ up to the axial position of the rear stagnation point, which is followed by a rapid decay, accords with the data available in separated flows (e.g. Durão & Whitelaw 1978; Crabb, Durão & Whitelaw 1981; Etheridge & Kemp 1978; Moss *et al.* 1979). Table 5 summarizes the maxima of the r.m.s. velocity fluctuations

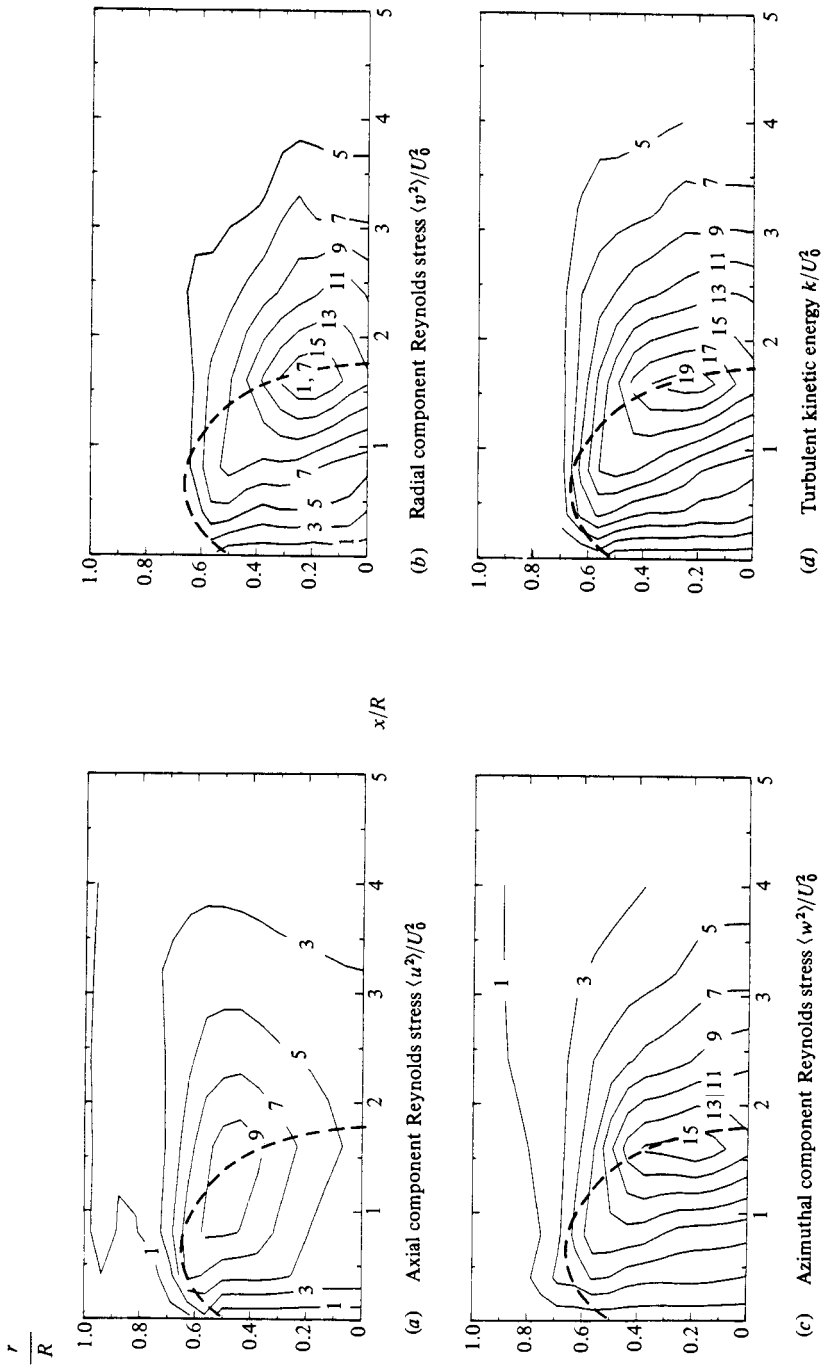

FIGURE 8. Disk, 25% blockage: contours of Reynolds stress (per cent ρU_0^2; $U_0 = 1.37$ m s^{-1}).
Broken line shows the locus of the separation streamline.

Authors	Flow type	$\frac{\langle u^2\rangle^{\frac{1}{2}}}{U_0}$	$\frac{\langle v^2\rangle^{\frac{1}{2}}}{U_0}$	$\frac{\langle w^2\rangle^{\frac{1}{2}}}{U_0}$
This paper	Confined disk, 25 % blockage	0.35	0.42	0.42
	Confined cone, 25 % blockage	0.30	0.28	0.33
	Confined disk, 50 % blockage	0.36	0.26	0.36
Fujii *et al.* (1978)	Confined wedge, 50 % blockage	$(\frac{2}{3}k)^{\frac{1}{2}}/U_0 \approx 0.26$		
Durão & Whitelaw (1978)	Annular jet, disk, 50 % blockage	0.30	0.30	0.25
Smyth (1979)	Wall-mounted disk	0.30	0.25	—
Bradbury (1976)	Flat plate, 10 % blockage	0.35	0.65	0.35
Castro & Robbins (1977)	Surface-mounted cube	0.28	—	—
Crabb *et al.* (1981)	Surface-mounted rib	0.40	—	—
Etheridge & Kemp (1978)	Backward-facing step	0.20	0.15	—
Moss *et al.* (1979)	Backward-facing step	0.19	0.14	0.18

Note that normalizing velocity U_0 is defined as follows:
(i) maximum value at trailing edge of baffle (Fujii *et al.* 1978; Durão & Whitelaw 1978);
(ii) approach velocity (Smyth 1979; Castro & Robbins 1977; Crabb *et al.* 1981);
(iii) freestream velocity (Bradbury 1976; Moss *et al.* 1979);
(iv) maximum axial velocity at given station (Etheridge & Kemp 1978).

TABLE 5. Maximum r.m.s. velocity fluctuations in various separated recirculating flows

which have been measured in a variety of separated recirculating flows, either by laser-Doppler velocimetry or pulsed-wire anemometry. The present results are similar to those reported by other workers, particularly when notice is taken of the different ways in which the normalizing velocity has been chosen: see the footnote to this table. The highest measured is the data of Crabb *et al.* (1981), which may be explained by their observation of bimodal probability distributions which imply the existence of preferred frequencies.

The development of $\langle v^2\rangle$ and $\langle w^2\rangle$ is markedly different from that of $\langle u^2\rangle$, with the maxima occurring very close to the rear stagnation point. As a result, the anisotropy of Reynolds stress on the centreline (figure 9) is particularly high. Comparison with many of the flows in Table 5 does not allow useful generalizations to be drawn, because similar behaviour is impossible in flows for which the rear stagnation point lies at a solid surface. Of the flows with free rear stagnation points, the qualitative behaviour of the contours on figure 8 is similar to the data of Durão & Whitelaw (1978), although the latter pertain to a higher blockage ratio. The unusually high value for $\langle v^2\rangle^{\frac{1}{2}}/U_0$ reported by Bradbury (1976), and given in table 5, was explained as the result of vortex shedding. We have already drawn attention to the absence of any discernible flow oscillations, and similar conclusions have been drawn by Durão & Whitelaw (1978) *within* the recirculation zone of an annular jet.

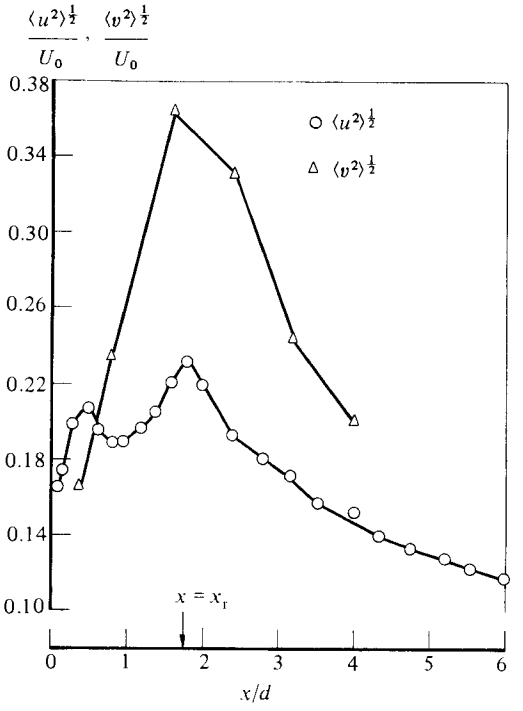

FIGURE 9. Disk, 25% blockage: centreline values of turbulence intensity. Recirculation zone length is marked by arrow on abscissa (U_0 = 1.37 m/s, d = 25.4 mm).

These results suggest the presence of alternative sources of the high values of $\langle v^2\rangle$, and one such is discussed in §4.

Cone, 25% blockage

The qualitative features of this flow (figure 10) are similar to those of the 25% blockage disk: $\langle v^2\rangle$ and $\langle w^2\rangle$ are largest close to the rear stagnation point, while the highest value of $\langle u^2\rangle$ lies at $r/R \approx 0.5$. The maxima of the Reynolds stresses are smaller (for example, the maximum turbulent kinetic energy is only 60% that of the disk), as is the centreline anisotropy shown on figure 11.

Disk, 50% blockage

Although the position and value of maximum $\langle u^2\rangle$ (figure 12*a*) is similar to the 25% blockage disk, this flow results in the maxima of $\langle v^2\rangle$ and $\langle w^2\rangle$ (figures 12*b*, *c*), being approximately coincident with that of $\langle u^2\rangle$, rather than on the centreline. It is noted that, for the contours of $\langle v^2\rangle$, the use of linear interpolation between data points at $0.6r/R$ and $0.7r/R$ results in an underestimation of the magnitude of $\langle v^2\rangle$ in this region. Because the development of each component is similar, with the largest values at a given axial station lying within the region of large axial velocity gradient, the shear layer resembles a simple mixing layer, although this resemblance is only qualitative since the turbulence levels here are very much higher. That the stresses are distributed in this way is presumably because of the elongated shape of the recirculation bubble caused by confinement. For this reason little similarity would be expected with the annular jet, measured by Durão & Whitelaw (1978), for a 50% blockage disk which resulted in a *shorter* recirculation zone than the present flow.

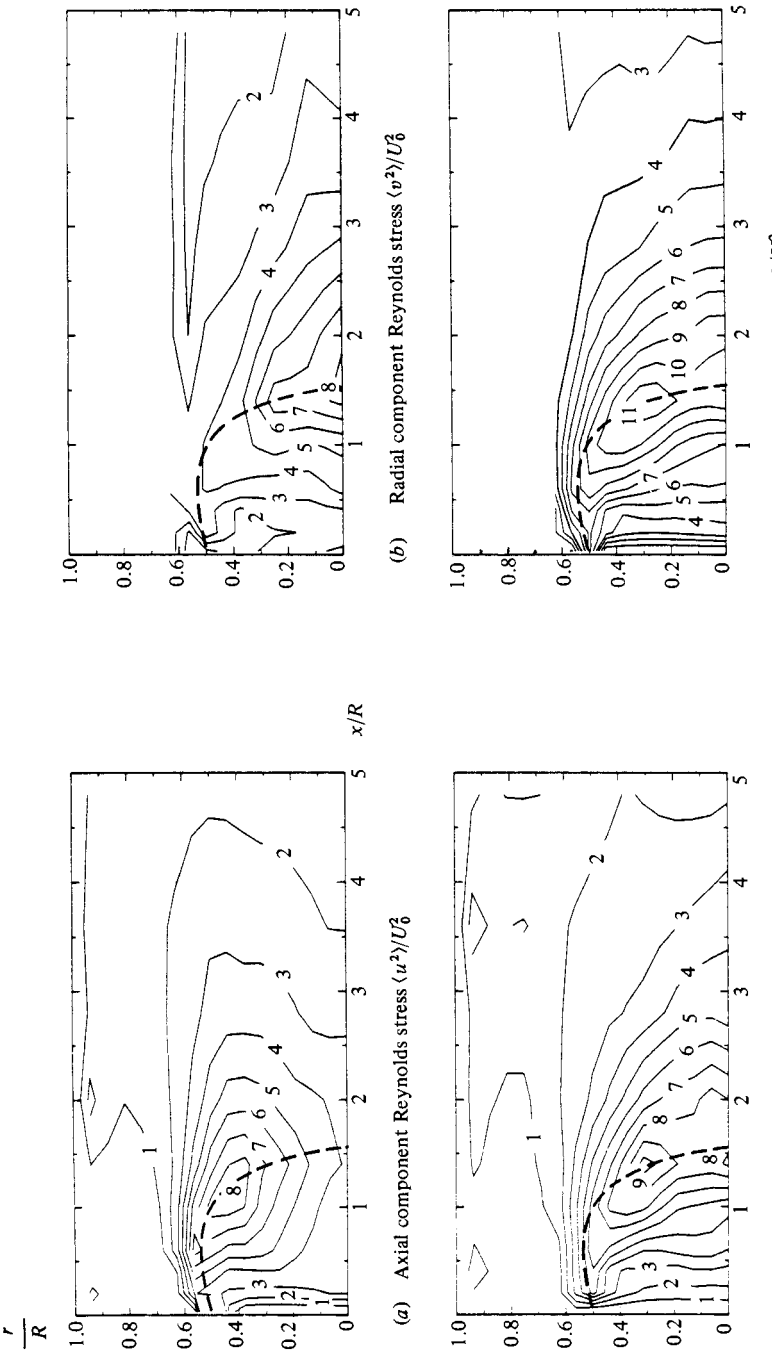

FIGURE 10. Cone, 25 % blockage: contours of Reynolds stress (per cent ρU_0^2; $U_0 = 1.53$ m s^{-1}). Broken line shows the locus of the separation streamline.

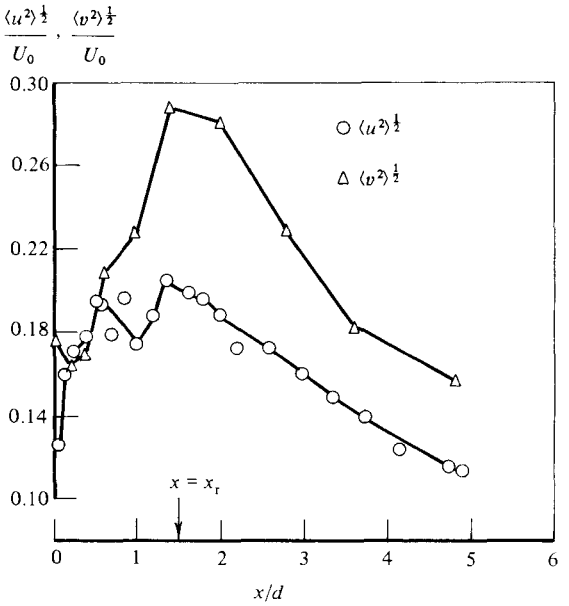

FIGURE 11. Cone, 25% blockage: centreline values of turbulence intensity. Recirculation zone length is marked by arrow on abscissa ($U_0 = 1.53$ m s^{-1}, $d = 25.4$ mm).

The maximum value of the turbulent kinetic energy is about $0.14U_0^2$, as compared with $0.18U_0^2$ for the 25% blockage disk. If the underestimation of $\langle v^2\rangle$ in the present flow is taken into account, it is likely that this difference is even smaller. However, the centreline partitioning of this energy is quite different, as exemplified by the approximate isotropy of the Reynolds stresses (figure 13).

4. Discussion

The aspects of the flow field that are of interest here are the size of the recirculation region, the recirculating mass-flow rate and the levels of turbulence which are generated. The following paragraphs examine the influence of the forebody shape and the blockage and the effect of confinement on these characteristics. Blockage refers to the area blockage presented by the baffle to the approaching stream. In the experiments of this paper, the flow downstream of the baffle is always confined by the pipe wall. The flow investigated by Durão & Whitelaw (1978) was, in contrast, unconfined downstream of the baffle, although the baffle still presented a blockage.

Table 4 compares the size of the recirculation zones and recirculating mass flow rates measured in this paper with those of other workers. Without exception (e.g. Davies & Béer 1971; Winterfeld 1965; Calvert 1967) it is found that decreasing bluffness gives rise to narrower and shorter recirculation bubbles with smaller recirculating mass-flow rates, although the magnitudes vary from reference to reference. The relative decrease in length between a disk and a 45° cone is, however, similar ($\approx 15\%$) in all references, as is that for $\dot{m}_r/\dot{m}$.

The magnitude of the maximum negative centreline axial velocity is smaller (figure 5) for the cone than for the disk. This velocity is interesting because it is a characteristic velocity of the recirculation zone and also because it influences the magnitude of the recirculating mass flow rate. Table 4 compares values of this

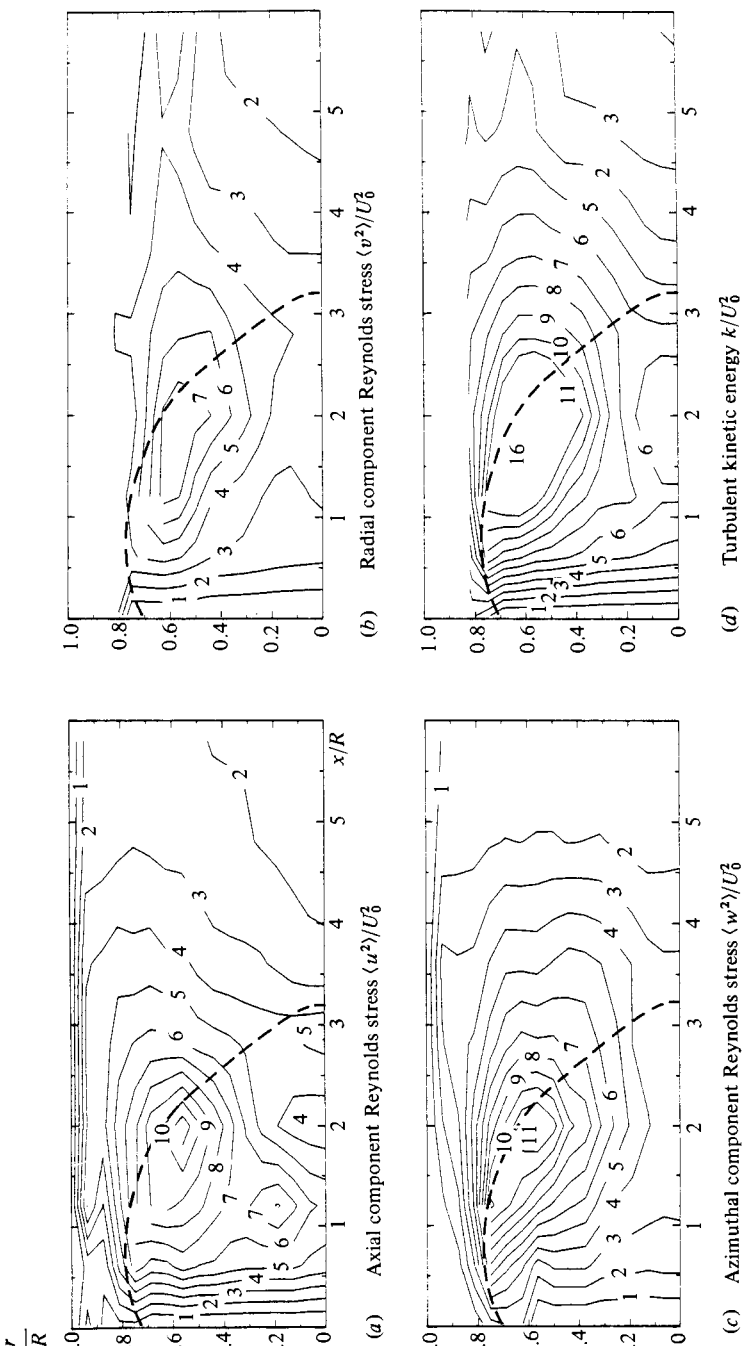

FIGURE 12. Disk, 50% blockage: contours of Reynolds stress (per cent ρU_0^2; $U_0^2 = 1.62$ m s^{-1}). Broken line shows the locus of the separation streamline.

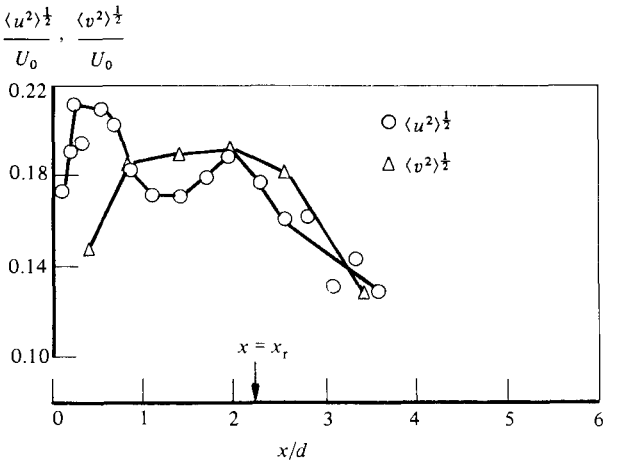

FIGURE 13. Disk, 50 % blockage: centreline values of turbulence intensity. Recirculation-zone length is marked by arrow on abscissa ($U_0 = 1.62$ m s^{-1}, $d = 35.6$ mm).

quantity and shows, for example, that the recirculating mass-flow rate behind the 25 % blockage cone is only 60 % of that of the equivalent disk. To explain the reason for the smaller velocity in the wake of the cone, it is necessary to outline how this flow comes about.

The flow streamlines, on separating from the baffle, undergo large curvature (e.g. the loci of the separation streamlines, figure 6), which is associated with pressure gradients that are directed normally to the streamlines: the magnitude of these gradients depends on the degree of curvature. As a result, a pressure minimum exists at the 'eye' of the recirculation bubble. Given the experimental observation that the streamline curvature is milder for the cone than for the disk (figure 6), the pressure at the eye in the case of the cone is larger than for the disk. Far downstream, the flows both recover to the same pressure, and hence the axial pressure gradients for the cone are smaller than for the disk. On the centreline, the acceleration of fluid is dominated by the magnitude of this pressure gradient, which, being relatively smaller for the cone, therefore gives rise to smaller centreline velocities.

Inspection of the contours of Reynolds stress for the disk and the cone (figures 8 and 10) reveals distributions that are qualitatively similar. This result is unsurprising, because the velocity fields, and hence the rates of strain, are also similar. The magnitudes of $\langle v^2\rangle$ and $\langle w^2\rangle$ (and less so $\langle u^2\rangle$) are smaller for the cone, by about one half and one third respectively, with the result that the centreline distribution of turbulent kinetic energy is found to be only 60 % that of the disk (figure 14). Because the shear layer surrounding the recirculation bubble is a region of intense generation of turbulence, these results can be explained by examination of some of the terms in the conservation equation for turbulent kinetic energy (see e.g. Bradshaw 1971).

Figure 15 shows the radial distribution of the terms representing net convection, production by normal stresses and production by shear stress for the disk of 25 % area blockage. The abscissa is in units of $\rho U_0^3/R$, and positive quantities represent a gain of energy. Profiles are presented for axial locations within the recirculation zone ($x/R = 0.4$), near the free stagnation point ($x/R = 1.6$) and in the wake proper ($x/R = 3.2$). The net convection and the production by normal stresses have been evaluated directly from the measurements, with the quotient V/r evaluated (from

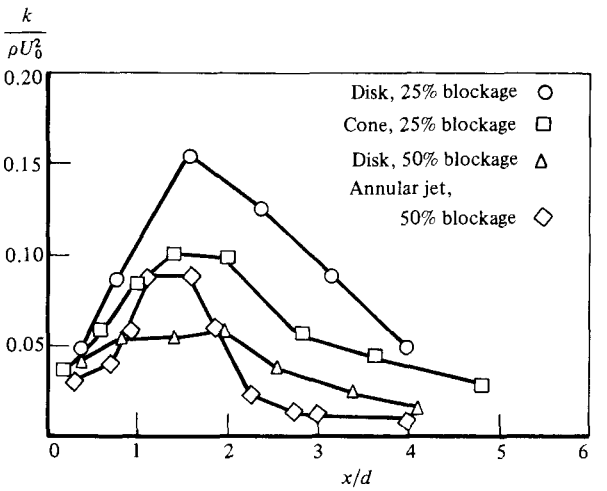

FIGURE 14. Centreline values of turbulent kinetic energy (lengthscale d is diameter of each baffle).

continuity) as $-\partial U/\partial x - \partial V/\partial r$, a practice that minimizes the influence of systematic experimental errors. It has not been possible to measure (or deduce) the Reynolds shear stress in these flows. We have, however, estimated this quantity by assuming a correlation coefficient for $\langle uv \rangle$ that varies linearly from a value of zero at the centreline to 0.5 at $r/R = 0.5$, followed by a linear decay to zero at the pipe wall. We therefore emphasize that the distributions are qualitative, although this is sufficient for our purpose, and note that the maximum value of the correlation coefficient is in accordance with the measurements of Etheridge & Kemp (1978) in a related flow.

The distribution of the terms upstream of the free stagnation point ($x/R = 0.4$) and near the separation streamline are similar to those of a simple mixing layer, in that convection and production (by shear stress) are large with convection representing a net loss. Given the nature of the assumptions made in finding production, no significance should be attached to the coincidence of radial position of the peaks of convection and production, something not observed in mixing layers. Within the recirculation zone, convection is the largest term, is comparatively uniformly distributed, and here represents a gain. Downstream of the recirculation zone ($x/R = 3.2$), convection is the dominant gain together with some shear-stress production at $r/R \approx 0.5$: such features are expected in wake flows. In the vicinity of the free stagnation point ($x/R = 1.6$), the flow retains its 'mixing-layer' characteristics for $r/R \gtrsim 0.4$. At smaller radii, however, production of turbulent kinetic energy *through the interaction of normal stresses with normal strain* is not only the largest single term, but is also comparable to the largest rate of production by shear stress at the same axial station.

This observation is unusual, and accounts for both the large value of $\langle v^2 \rangle$ and $\langle w^2 \rangle$ near the free stagnation point and the large anisotropy between $\langle v^2 \rangle$ and $\langle u^2 \rangle$ since, although production of the former represents a gain, 'production' of $\langle u^2 \rangle$ is $-2\langle u^2 \rangle \partial U/\partial x$, which is a negative quantity, a *loss*. The distributions for the cone (not presented) show the same qualitative features and, in particular, confirm the importance of the generation of turbulent kinetic energy through normal stresses. For the larger disk (also not presented) the value of $\partial U/\partial x$ near the rear stagnation point

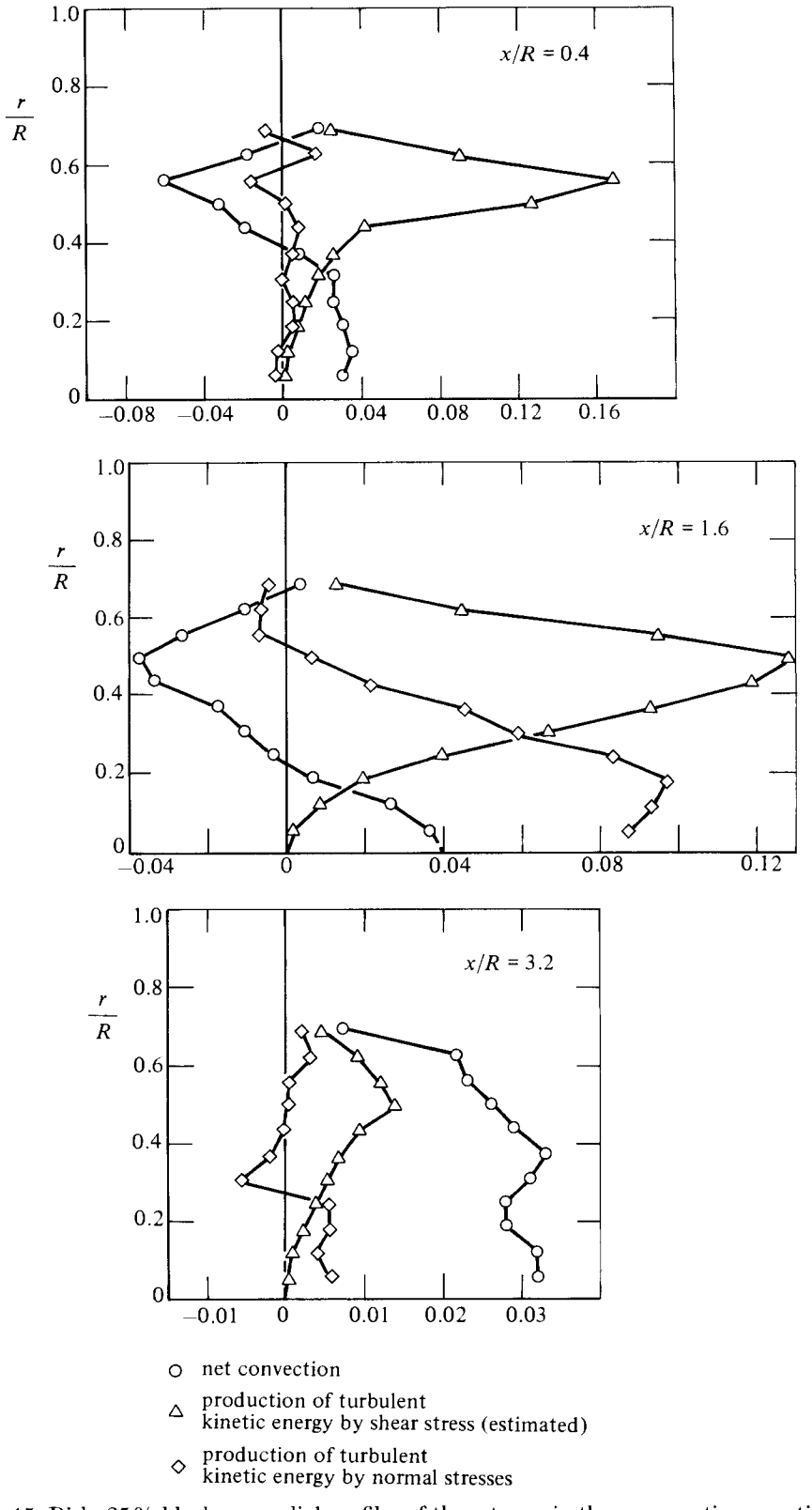

FIGURE 15. Disk, 25% blockage: radial profiles of three terms in the conservation equation for turbulent kinetic energy. Abscissa in units of $\rho U_0^3/R$.

is comparatively smaller, owing to the longer recirculation region, and the contribution to production through normal stresses is an unimportant term in the balance.

For those flows in which there is large production of turbulent kinetic energy through the normal stress near the free stagnation point, calculations using a scalar effective-viscosity turbulence model (e.g. the 'k-ϵ' model) will be inaccurate, at least for the turbulence near the rear stagnation point. This is because such models do not adequately represent normal stresses and our experience with attempts to calculate these flows (McGuirk, Taylor & Whitelaw 1982; Taylor 1981) confirms this. Although the gradients of normal stress (where 'normal' now refers to streamline coordinates) are not large terms in the transport of mean momentum, the importance of the various production terms in generating turbulent kinetic energy implies that it is necessary to calculate the individual normal stresses adequately (using an appropriate turbulence model) if the correct turbulent kinetic energy is to be obtained. This distribution is crucial to the correct representation of the effective viscosity, and the latter quantity *is* of importance in the mean momentum equations.

The importance of turbulent exchange between the recirculating and surrounding flow in flame stabilization has been mentioned in §1. Taking turbulent kinetic energy as a measure of the exchange, the contour levels on figures 8 and 10 show that this is higher for the disk than for the cone. This is in agreement with Winterfeld's (1965) measurements for the residence time of a passive scalar in the recirculation bubble.

On increasing the blockage of the disk from 25% to 50%, the angles of the streamlines at the trailing edge of the baffle (figure 4) are substantially reduced. This results in a maximum width which is also reduced (table 4), but the length of the recirculation bubble has increased by about one quarter. Table 4 shows that, although all previous measurements have shown the same dependence of width with blockage, the *opposite* trend for the length has been found; that is, the recirculation length becomes shorter with increasing blockage, irrespective of whether the flow is confined or not. Observations in confined axisymmetric flows have been, however, restricted to blockage less than 25%.

The increased length and decreased width of the recirculation bubble correspond to decreased streamline curvature, particularly downstream of the location of the maximum bubble width (see figure 6). The reason for this is the greater proximity of the separation streamline to the pipe wall as compared with the 25% blockage disk. As a consequence the generation of large velocity components in the direction normal to the wall, which would be required for large curvature, is inhibited. The distance of the separation streamline from the wall is closely related to the distance of the baffle tip from the wall. It is noted that changing from 25% to 50% blockage, in axisymmetric flows, corresponds to the baffle diameter increasing from $0.5R$ to $0.71R$, whereas the same change in blockage in a plane geometry results in increasing the width of the baffle from $0.25R$ to $0.50R$. The influence of area blockage on, say, recirculation length can thus be expected to be substantially weaker in plane geometries and this is confirmed by comparing the measurement of Fujii *et al.* (1978) with that of Bradbury (1976), given in table 4.

The decrease in streamline curvature, noted in the previous paragraph, might have been thought to result in a smaller minimum pressure in the eye of the recirculation bubble than for the 25% area blockage disk and hence correspondingly smaller reversed velocities on the centreline. However, figure 5 shows that the converse is true; that is, the reversed velocities are larger for the 50% area blockage disk. These stem from the lower value of pressure which occurs behind the larger disk owing to the larger values of velocity outside the separation streamline as the maximum bubble

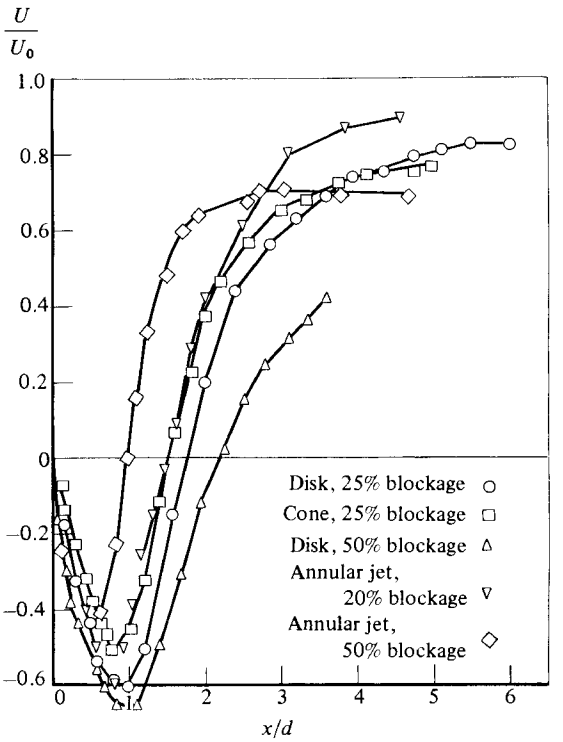

FIGURE 16. Centreline profiles of axial velocity for confined flows and annular jets (lengthscale d is diameter of each baffle).

width is approached (see figure 2.18 of Taylor 1981), which are accompanied by increased centripetal forces (and hence increased pressure gradients). The observation that the dimensionless recirculating mass-flow rate is smaller for this case than for the 25% blockage disk has already been noted and explained in §3.1.

The increased length of the recirculation zone results in a qualitatively different distribution of the Reynolds stresses as compared with the smaller baffles. Figure 5 shows that the centreline value of $\partial U/\partial x$ is smaller than for the 25% blockage disk, and so, according to the arguments presented above, the importance of normal-stress–normal-strain interactions is reduced, giving rise to the small anisotropy of figure 13. A further result of the reduced centreline production of $\langle w^2 \rangle$ is the low value of the centreline turbulent kinetic energy, shown on figure 14. Turbulent production is thus principally restricted to the shear layer surrounding the separation streamline, close to the location of the greatest width of the recirculation bubble. This, however, should not be taken to imply that the entire production of kinetic energy is by the interaction of shear stress and shear strain $\langle uv \rangle \partial U/\partial r$ alone. If this were so, then the maximum value of $\langle u^2 \rangle$ would be greater than that of $\langle v^2 \rangle$ and $\langle w^2 \rangle$, and this is not observed to be the case.

The influence of a confining wall on the flow downstream of a baffle, as opposed to one in which the downstream flow is free (such as an annular jet), can be explained on the basis of the above description of the flow development. Whether confined or not, table 4 shows that decreasing forebody bluffness results in narrower, shorter recirculation zones, because the angle of separation becomes smaller in both cases.

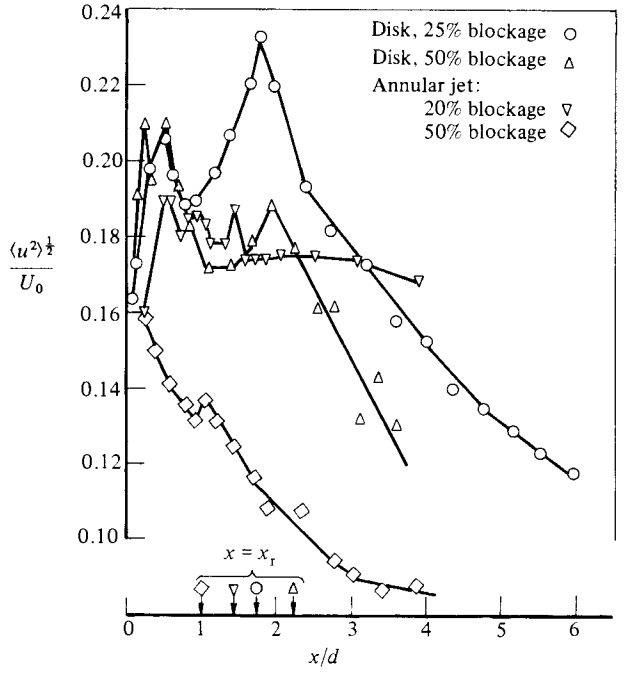

(*a*)

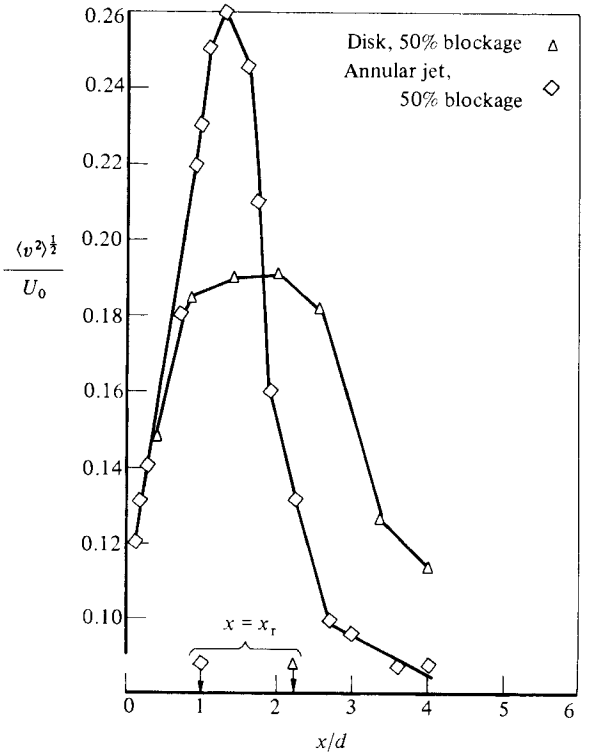

(*b*)

FIGURE 17. (*a*) Centreline values of axial turbulence intensity for confined flows and annular jets. Recirculation-zone lengths marked by arrows on abscissa. (*b*) Centreline values of radial turbulence intensity for confined flows and annular jets. Recirculation-zone lengths marked by arrows on abscissa.

The dimensionless lengths of the recirculation bubble are for a given blockage, however, consistently larger in the case of confined flows as compared with annular jets. There are two obvious influences that a confining wall exerts in this connection. The first is that it prevents the development of large streamline curvature towards the axis of symmetry as explained above for the effect of increasing area blockage ratio. The second is that it maintains the existence of positive velocities of the order of U_0 at all downstream stations, which is not the case in an annular jet because of the diffusion of axial momentum away from its outer edge. In the confined case, therefore, the larger positive velocities are better able to overcome the adverse pressure gradients, thereby giving rise to longer recirculation zones.

Comparison of the results of this work and those of Durão & Whitelaw (1978) reveals the effect of confinement on the Reynolds stresses. Figure 14 shows that the annular jet of 50% blockage gives rise to higher centreline turbulent kinetic energy than the equivalent confined flow near the free stagnation point. Examination of the development of the centreline axial velocity (figure 16) shows that $\partial U/\partial x$ is larger in this region for the unconfined flow which leads to the expectation of low $\langle u^2 \rangle$ and high $\langle w^2 \rangle$ in the annular jet flow as compared to the confined flow. Figures 17 (*a*, *b*) confirm this.

5. Summary

The following is a summary of the more important findings and conclusion of this work.

1. The influence of baffle forebody shape, on changing from a disk to a 45° cone of 25% blockage is to:
   (*a*) shorten and narrow (by about 10%) the recirculation bubble;
   (*b*) decrease (by 40%) the recirculating mass flow rate;
   (*c*) reduce (by 40%) the largest value of turbulent kinetic energy.
2. The influence of baffle blockage, on changing from a disk of 25% to 50% blockage is to:
   (*a*) lengthen (by about 25%) and narrow (by about 10%) the recirculation bubble;
   (*b*) decrease (by 16%) the dimensionless recirculating mass-flow rate;
   (*c*) reduce (by about 16%) the largest value of turbulent kinetic energy.
3. The measurements include the velocity characteristics both upstream of, and in, the plane of the trailing edge of the baffles which are useful as boundary conditions in numerical solutions of the equations of motion. In this plane, the decrease in bluffness (see (1) above) is accompanied by a halving of the radial velocities and the increase in blockage (see (2) above) reduces the streamline angles.
4. The decrease in the length and width of the recirculation bubble with diminishing bluffness is the result of decreased streamline angles at the trailing edge of the baffle.
5. The increase in recirculation length for blockage above 25% is opposite to the trend in unconfined flows. The difference is due to the confining wall both preventing the generation of large streamline curvature towards the rear stagnation point and maintaining large axial velocities at all downstream stations.
6. The distribution of the Reynolds stresses changes markedly with the increase in blockage: for the 25% blockage disk the maximum turbulent kinetic energy lies near the rear stagnation point, whereas for the 50% blockage disk it is far from the centreline, in the shear layer. Examination of the terms in the transport equation

for turbulent kinetic energy shows that, for the smaller disk, production by the normal stresses is an important contribution to the overall balance in this region.

We are pleased to be able to acknowledge many useful discussions with Dr J. J. McGuirk. We are grateful to the Science and Engineering Research Council for financial support of this work.

REFERENCES

BRADBURY, L. J. S. 1976 Measurements with a pulsed-wire and a hot-wire anemometer in the highly turbulent wake of a normal flat plate. *J. Fluid Mech.* **77**, 473–497.

BRADSHAW, P. 1971 *An Introduction to Turbulence and its Measurement.* Pergamon.

CALVERT, J. R. 1967 Experiments on the low-speed flow past cones. *J. Fluid Mech.* **27**, 273–289.

CARMODY, T. 1964 Establishment of the wake behind a disc. *Trans. ASME* D: *J. Basic Engng* **86**, 869–882.

CASTRO, I. P. & ROBINS, A. G. 1977 The flow around a surface-mounted cube in uniform and turbulent streams. *J. Fluid Mech.* **79**, 307–335.

CHIGIER, N. A. & GILBERT, J. L. 1968 Recirculation eddies in the wake of flameholders. *J. Inst. Fuel*, **41**, 105–113.

CRABB, D., DURÃO, D. F. G. & WHITELAW, J. H. 1981 Velocity characteristics in the vicinity of a two-dimensional rib. Paper presented at *3rd Symp. on Turbulent Shear Flows, Davis, California, 9–11 September 1981.*

DAVIES, T. W. & BÉER, J. M. 1971 Flow in the wake of bluff-body flame stabilisers. In *Proc. 13th Symp (Intl) on Combustion*, pp. 631–638. Combustion Institute, Pittsburgh.

DURÃO, D. F. G., FOUNTI, M. & WHITELAW, J. H. 1979 Velocity characteristics of three-dimensional disc-stabilised diffusion flames. *Lett. Heat Mass Transfer* **6**, 1–13.

DURÃO, D. F. G. & WHITELAW, J. H. 1978 Velocity characteristics of the flow in the near wake of a disk. *J. Fluid Mech.* **85**, 369–385.

DURST, F., MELLING, A. & WHITELAW, J. H. 1981 *Principles and Practice of Laser-Doppler Anemometry*, 2nd edn. Academic.

ETHERIDGE, D. W. & KEMP, P. H. 1978 Measurements of turbulent flow downstream of a rearward-facing step. *J. Fluid Mech.* **86**, 545–566.

FAIL, R., LAWFORD, J. A. & EYRE, R. C. W. 1957 Low speed experiments on the wake characteristics of flat plates normal to an air stream. *Min. of Supply, R. & M.* no. 3120, *RAE Rep. Aero.* 25160.

FUJII, S., GOMI, M. & EGUCHI, K. 1978 Cold flow tests of a bluff-body flame stabilizer. *Trans. ASME* I: *J. Fluids Engng* **100**, 323–333.

GEORGE, W. K. & LUMLEY, J. L. 1973 The laser-Doppler velocimeter and its application to the measurement of turbulence. *J. Fluid Mech.* **60**, 321.

HUMPHRIES, W. & VINCENT, J. H. 1976*a* Experiments to investigate transport processes in the near wakes of disks in turbulent air flow. *J. Fluid Mech.* **75**, 737–749.

HUMPHRIES, W. & VINCENT, J. H. 1976*b* Near wake properties of axisymmetric bluff body flows. *Appl. Sci. Res.* **32**, 649–669.

KIRMSE, R. 1974 Optische Probleme bei der Anwendung des Laser-Doppler Anemometers zur Messung von Strömungsgeschwindigkeiten in Flüssigkeiten. *Arch. f. tech. Messen*, Blatt V, 1246–1.

MCGUIRK, J. J., TAYLOR, A. M. K. P. & WHITELAW, J. H. 1982 The assessment of numerical diffusion in upwind difference calculations of turbulent recirculating flows. In *Turbulent Shear Flows 3* (ed. L. J. S. Bradbury *et al.*), pp. 206–224. Springer.

MOSS, W. D., BAKER, S. & BRADBURY, L. J. S. 1979 Measurements of mean velocity and Reynolds stresses in some regions of recirculating flow. In *Turbulent Shear Flows I* (ed. F. Durst *et al.*), pp. 198–207. Springer.

SMYTH, R. 1979 Turbulent flow over a disk normal to a wall. *Trans. ASME* I: *J. Fluids Engng* **101**, 461–466.

SULLEREY, R. K., GUPTA, A. K. & MOORTHY, C. S. 1975 Similarity in the turbulent near wake of bluff bodies. *AIAA J.* **13**, 1425–1430.

TAYLOR, A. M. K. P. 1981 Confined, isothermal and combusting flows behind axisymmetric baffles. Ph.D. Thesis, University of London.

WINTERFELD, G. 1965 On processes of turbulent exchange behind flame holders. In *Proc. 10th Symp. (Intl) on Combustion*, pp. 1265–1275. Combustion Institute, Pittsburgh.